

Chaos in the relativistic cyclotron motion of a charged particle

Jung-Hoon Kim and Hai-Woong Lee

Department of Physics, Korea Advanced Institute of Science and Technology, Taejeon 305-701, Korea

(Received 10 May 1996)

The relativistic dynamics of a charged particle moving in a uniform magnetic field and a time-periodic electric field is investigated. It is shown that various features such as nonlinear resonances, stochastic layers near resonance separatrices, bifurcations of fixed points, and reconnection phenomena can be exhibited by the particle when the relativistic effect becomes appreciable. [S1063-651X(96)05210-5]

PACS number(s): 05.45.+b, 03.30.+p, 29.20.Hm, 47.20.Ky

I. INTRODUCTION

The subject of chaos has drawn considerable attention in the past, due to the perception that complex behavior in the motion of a system can be caused by rather simple governing equations [1]. In most systems examined in the past, the source of the chaotic behavior is nonlinear interaction terms in the equations of motion. The quadratic response to the environment in the logistic model of population growth, the cubic restoring force in the Duffing oscillator, and nonlinear coupling in the coupled oscillators are a few examples which serve as physical origins for the complicated and stochastic behavior of the model systems.

In recent papers it was reported that relativistic mass effects can make systems behave in significantly different manners from those displayed by the corresponding systems governed by nonrelativistic Newtonian equations of motion [2–8]. Even the driven harmonic oscillator, a standard textbook example of a system with a linear interaction, has been shown to exhibit chaos when relativistic effects are considered [7]. The source of the complex relativistic behavior in these cases lies in the nonlinearity from the relativistic kinetic energy term in the Hamiltonian. This relativistic nonlinearity can be considered properly when the motion of a system becomes relativistic. The main purpose of the present study is to illustrate the consequence of the relativistic effects using a simple and practically important model system, where the relativistic nonlinearity results in a chaotic behavior that is absent in the corresponding nonrelativistic system.

A charged particle moving in a constant magnetic field, and an electric field oscillating in the plane perpendicular to the magnetic field, can provide such a simple model. From the early history of accelerators, this system has been considerably studied. In the framework of nonrelativistic Newtonian mechanics, when the frequency of the electric field is set at the particle's cyclotron frequency, the particle can be accelerated without limits. In reality, however, due to the relativistic mass effect, the orbital phase of the particle motion lags increasingly behind the phase of the electric field, as the particle energy is increased. A continuous change in the frequency of the electric field to lower values is thus required if resonance is to be maintained [9]. In this paper we show that if the frequency of the electric field is fixed, various interesting features such as nonlinear resonances, stochastic layers near separatrices, bifurcations of fixed points, and reconnection phenomena can be exhibited by the system

when the relativistic effects become appreciable.

Extensive studies have been made during the last few decades on a charged particle in a uniform magnetic field interacting with an electromagnetic wave [10–14]. The onset of chaos was detected in such a system in both relativistic and nonrelativistic regimes, chaotic behaviors being somewhat varied in their details. The present system considered here differs from those studied earlier, in that it is completely integrable in the nonrelativistic regime. There is no nonlinearity other than that arising from the kinetic energy term in the Hamiltonian, and thus any chaotic behavior exhibited by our system is due solely to the relativistic effects.

II. REDUCTION TO THE ONE-DEGREE-OF-FREEDOM PROBLEM

We consider a charged particle of mass m and charge q immersed in a uniform magnetic field $\mathbf{B} = B\mathbf{e}_z$ moving under the influence of a periodic driving electric field $\mathbf{E}(t) = E_0 \cos \omega t \mathbf{e}_y$. The relativistic equation of motion for the particle is given by [9]

$$\frac{d}{dt} \left[\frac{m\mathbf{v}}{\sqrt{1-v^2/c^2}} \right] = q\mathbf{v} \times \mathbf{B} + q\mathbf{E}(t). \quad (1)$$

The right hand side of the above equation represents the Lorentz force exerted on the charged particle, and the term $m/\sqrt{1-v^2/c^2}$ in the brackets represents the relativistic mass. In terms of mechanical momentum $\mathbf{p} = m\mathbf{v}/\sqrt{1-v^2/c^2}$, Eq. (1) can be written by components as

$$\frac{dp_x}{dt} = \frac{qBp_y}{\sqrt{m^2 + p^2/c^2}}, \quad (2)$$

$$\frac{dp_y}{dt} = -\frac{qBp_x}{\sqrt{m^2 + p^2/c^2}} + qE_0 \cos \omega t, \quad (3)$$

$$\frac{dp_z}{dt} = 0. \quad (4)$$

We note that there are no terms depending on coordinate variables in Eqs. (2)–(4), and thus all information on the dynamics of the particle can be obtained by inspecting the system in momentum space. A further reduction in the di-

mension of the phase space can be achieved by noting that the z component of the momentum is conserved. Introducing the effective mass m_e as

$$m_e^2 = m^2 + p_z^2/c^2, \quad (5)$$

we immediately see that the motion of the particle can be described in the two-dimensional phase space by Eqs. (2) and (3), with m replaced by m_e and $p = \sqrt{p_x^2 + p_y^2}$ interpreted as the distance from the origin in that phase space. At this point it is worthwhile to note that the effective mass, which plays the role of the mass of the particle in the prescribed two-dimensional phase space, arises solely from the relativistic consideration. In the nonrelativistic limit, $c \rightarrow \infty$, the effective mass m_e equals the rest mass m , as can be seen from Eq. (5).

Let us now introduce an equivalent one-degree-of-freedom Hamiltonian for our particle. If we denote p_x and p_y by Q and P , respectively, the equations of motion for our particle can be written as

$$\frac{dQ}{dt} = \frac{\Omega_0 P}{\sqrt{1 + (Q^2 + P^2)/m_e^2 c^2}}, \quad (6)$$

$$\frac{dP}{dt} = -\frac{\Omega_0 Q}{\sqrt{1 + (Q^2 + P^2)/m_e^2 c^2}} + qE_0 \cos \omega t, \quad (7)$$

where $\Omega_0 = qB/m_e$ is the nonrelativistic cyclotron frequency of the particle of mass m_e and charge q undergoing circular motion in a uniform magnetic field B . It is then immediately clear that Eqs. (6) and (7) can be derived from the Hamiltonian

$$H(P, Q) = \Omega_0 m_e^2 c^2 \sqrt{1 + (Q^2 + P^2)/m_e^2 c^2} - QqE_0 \cos \omega t. \quad (8)$$

It should be noted that, although our coordinate Q and momentum P represent two orthogonal components of mechanical momentum, they are canonically conjugate to each other, as shown in the Appendix.

In the absence of the driving electric field, Eqs. (6) and (7) can be easily solved to yield the solutions

$$Q(t) = \sqrt{Q_0^2 + P_0^2} \sin\left(\frac{\Omega_0}{\gamma} t + \phi_0\right), \quad (9)$$

$$P(t) = \sqrt{Q_0^2 + P_0^2} \cos\left(\frac{\Omega_0}{\gamma} t + \phi_0\right), \quad (10)$$

where Q_0 and P_0 are the initial values of the canonical variables Q and P , respectively, and

$$\gamma = \sqrt{1 + (Q_0^2 + P_0^2)/m_e^2 c^2}, \quad (11)$$

$$\phi_0 = \tan^{-1}(Q_0/P_0). \quad (12)$$

We find from Eqs. (9) and (10) that the relativistic particle moves along a circle of radius $\sqrt{Q_0^2 + P_0^2}$ with frequency Ω_0/γ .

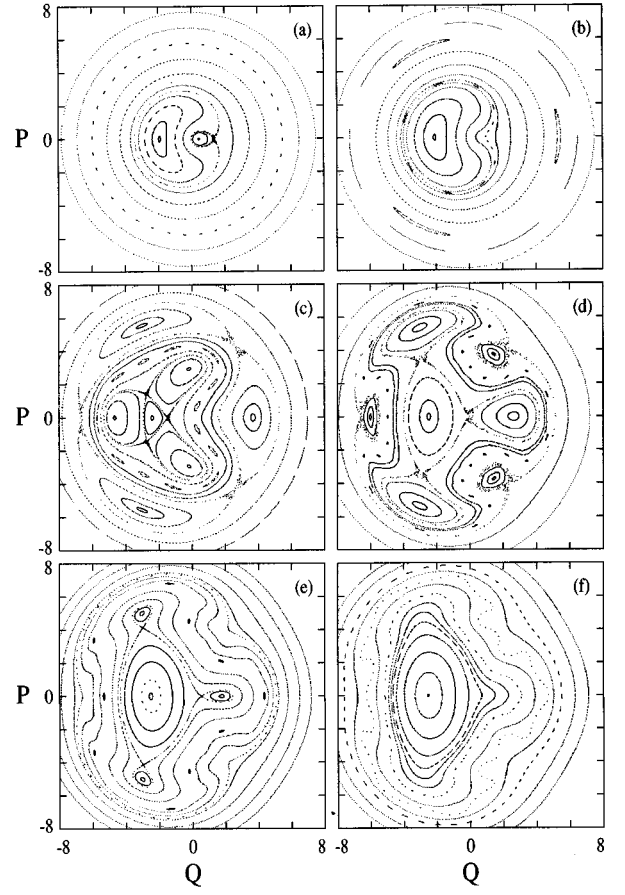


FIG. 1. Phase-space maps of the Hamiltonian (8) for the parameter values $m_e=1$, $q=1$, $c=1$, $\Omega_0=1$, and $\omega=0.5$ (in arbitrary units). The amplitude of the driving electric field E_0 is 0.3 for (a), 0.6 for (b), 1.8 for (c), 2.2 for (d), 2.4 for (e), and 2.6 for (f).

Before leaving this section, we remark that, in the nonrelativistic limit $c \rightarrow \infty$, the Hamiltonian given by Eq. (8) reduces to

$$H(P, Q) = \frac{\Omega_0}{2} P^2 + \frac{\Omega_0}{2} Q^2 - QqE_0 \cos \omega t, \quad (13)$$

which is just the Hamiltonian describing a driven simple harmonic oscillator, a completely integrable system, with mass $1/\Omega_0 = m/qB$ and spring constant $\Omega_0 = qB/m$. Thus the present system, in the nonrelativistic limit, exhibits regular dynamics without any complex behavior.

III. NUMERICAL SOLUTIONS OF THE EQUATIONS OF MOTION

If the relativistic effects are fully taken into account, the situation becomes fundamentally different from that of the nonrelativistic system. Numerical integrations of Eqs. (6) and (7) enable us to obtain the phase-space maps shown in Fig. 1. All the figures are drawn at the parameter values $m_e=1$, $q=1$, $c=1$, $\Omega_0=1$, and $\omega=0.5$ (in arbitrary units), while the amplitude of the driving electric field E_0 is varied. A variety of features that are normally attributed to a broad class of nonlinear systems can be observed in the present system. For instance, nonlinear resonances, stochastic layers

near the separatrices of resonance islands, bifurcations of fixed points, and reconnection phenomena can be observed through a close inspection of Fig. 1. Detailed descriptions of the observation are given below.

From Fig. 1(a), drawn at $E_0 = 0.3$, we can clearly see the period-1 resonance with an elliptic fixed point ($Q \cong -1.94$, $P = 0$) in the center of the island and a hyperbolic fixed point ($Q \cong 1.3$, $P = 0$) on the island boundary. As is well known [10,15], a primary period- n resonance occurs at the energy E_{nm} , satisfying the resonance condition

$$n\Omega(E_{nm}) = m\omega, \quad (14)$$

where n and m are integers, and Ω is the frequency of the motion of the unperturbed system. For our system described in Sec. II, $\Omega = \Omega_0/\gamma$. We note that, if the potential is symmetric, $V(-q) = V(q)$, only the odd-period resonances ($n = \text{odd}$) are of importance. Furthermore, if the driving force varies sinusoidally with time, only the primary resonances with $m = 1$ are of importance.

A close inspection of the phase-space map near the hyperbolic fixed point can reveal a possible stochastic behavior of the system. If a resonance island has a hyperbolic fixed point on its boundary, the frequency of the local rotational motion around the elliptic fixed point decreases as the separatrix is approached, and becomes zero on the separatrix. Resonances between this frequency and the driving frequency lead to the formation of an infinite number of second-order resonance islands in the neighborhood of the separatrix, inducing very complicated motions nearby. This qualitatively demonstrates the existence of the stochastic layer near a separatrix [10,15]. The stochastic layer, however, is bounded by surrounding Kol'mogorov-Arnol'd-Moser (KAM) curves at $E_0 = 0.3$.

Between the two fixed points above mentioned, there appears a period-1 fixed point ($Q \cong 0.44$, $P = 0$) the origin of which is basically different in nature from the other fixed points belonging to the resonance. If the amplitude of the driving electric field E_0 decreases to zero, this period-1 fixed point collapses into the point of phase space where the system has minimum energy, and in the present case this point corresponds to the center of the phase space. For this reason, we refer to this fixed point as the central fixed point. If we increase E_0 , the central fixed point approaches and eventually collides with the period-1 hyperbolic fixed point. After the collision, the two fixed points disappear via an inverse saddle node bifurcation, leading to a disappearance of the hyperbolic fixed point of the period-1 resonance island, as can be seen from Fig. 1(b). Without the hyperbolic fixed point on its boundary, the period-1 resonance island becomes free of chaos near the separatrix [12]. In Sec. IV, we theoretically calculate the critical value of E_0 at which this bifurcation phenomenon occurs.

Figure 1(c) implies that yet another kind of bifurcation has occurred. There emerge two period-3 resonance islands, a primary resonance occupying the outer region of phase space, and a second-order resonance occupying the inner region of phase space. The primary period-3 resonance exists for all nonzero values of E_0 , although its existence can barely be observed at small E_0 due to the fact that the width of the resonance island approaches zero as $E_0 \rightarrow 0$. In con-

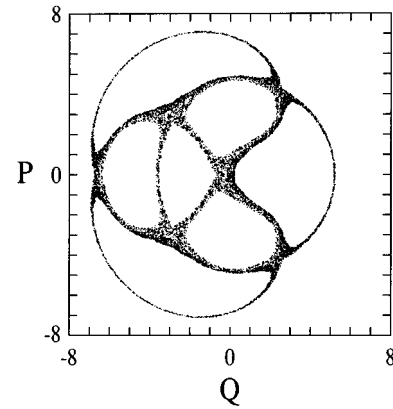


FIG. 2. Same as Fig.1, except $E_0 = 2.0$. One initial condition is taken.

trast, the second-order period-3 resonance has bifurcated out of the elliptic fixed point of the primary period-1 resonance at some critical value of E_0 . This critical value shall be estimated shortly in Sec. IV. At $E_0 = 1.8$, at which Fig. 1(c) was drawn, the second-order period-3 resonance island is clearly separated from the period-1 elliptic fixed point, and its width is already comparable to that of the primary period-3 resonance. We should emphasize that there still exist many KAM curves between the two period-3 resonances.

As E_0 grows to 2.2, there occurs a great change in the topology of the phase space as shown in Fig. 1(d). The KAM curves dividing the two period-3 resonance islands have vanished, and there appear invariant curves of different type dividing other parts of the phase space. This phenomenon, known as reconnection [16–18], involves the merging of two separatrices. Since there always exists a stochastic layer near the separatrix of the resonance island which has a hyperbolic fixed point on its boundary, one may suggest that, when two resonances undergo reconnection via separatrix merging, there should be stochastic orbits wandering along both separatrices. We show one such orbit in Fig. 2 which was drawn for a single initial condition at $E_0 = 2.0$. This stochastic behavior can be viewed to occur as a result of the overlap of two neighboring resonances [15]. As is widely understood, the resonance overlap is synonymous with global chaos because, when two resonance islands overlap with each other, one orbit that is stochastically wandering in the neighborhood of a resonance's separatrix can jump into the neighborhood of another resonance's separatrix, and then jump back at some later time. However, a reconnection differs from a resonance overlap in that, in the former case, the stochastic motion along the two separatrices is interrupted after another type of invariant curve builds up, as can instantly be seen from Fig. 1(d). In addition, during the reconnection one of the two heteroclinic orbits transforms into a homoclinic orbit [16–18] [compare Fig. 1(c) with Fig. 1(d)].

Finally, a further increase in E_0 causes the elliptic and hyperbolic fixed points of the second-order period-3 resonance to approach each other and to disappear in pair via the inverse saddle node bifurcation after the collision as shown in Fig. 1(e). The elliptic and hyperbolic fixed points of the primary period-3 resonance are bound to subsequently encounter the same fate, as can be seen in Fig. 1(f).

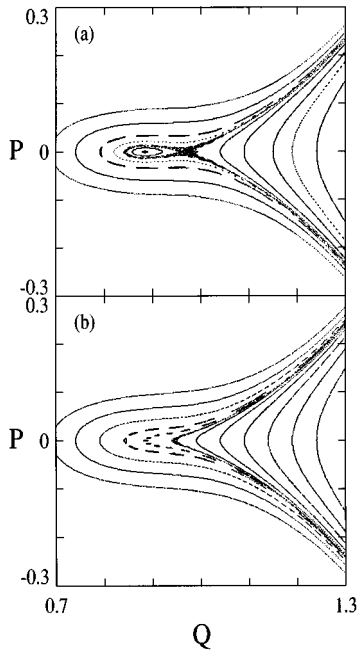


FIG. 3. Phase-space maps near the bifurcation point for the same parameters as in Fig. 1. The amplitude of the driving electric field E_0 is 0.432 for (a), and 0.434 for (b).

IV. THEORETICAL ANALYSIS

For our theoretical analysis, it is convenient to carry out a canonical transformation into the action-angle space. If we denote the action and angle variables for the unperturbed Hamiltonian by I and θ , respectively, the one-degree-of-freedom Hamiltonian derived in Sec. II can be written as

$$\begin{aligned}
 H(I, \theta) &= H_0(I) - qE_0\sqrt{2I}\cos\theta \cos\omega t \\
 &= \Omega_0 m_e c \sqrt{2I + m_e^2 c^2} - qE_0\sqrt{I/2} \\
 &\quad \times [\cos(\theta - \omega t) + \cos(\theta + \omega t)]. \tag{15}
 \end{aligned}$$

Let us first consider the critical value of E_0 at which the central fixed point and the period-1 hyperbolic fixed point collapse against each other. Through numerical computation, we determine this value to be $E_0 = 0.433$. Shown in Figs. 3(a) and 3(b) are the phase-space maps just below and above this value of E_0 . In order to calculate this value theoretically, we temporarily ignore the second term in the brackets of Eq. (15) which oscillates quickly, and perform a canonical transformation with the generating function

$$F_2(J, \theta) = J(\theta - \omega t). \tag{16}$$

The new Hamiltonian H' , expressed in terms of the slow variables

$$\psi = \theta - \omega t, \tag{17}$$

$$J = I, \tag{18}$$

takes the form

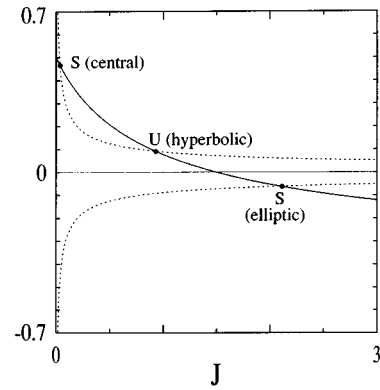


FIG. 4. Graphical solution of Eq. (22) showing fixed points and their stability for the parameters $m_e = 1$, $q = 1$, $c = 1$, $\Omega_0 = 1$, $\omega = 0.5$, and $E_0 = 0.25$ (in arbitrary units). The solid curve corresponds to $1/(\sqrt{2J+1}) - 0.5$, and the dotted curves correspond to $\pm(E_0/2\sqrt{2J})$. S and U represent stable and unstable fixed points, respectively.

$$H'(J, \psi) = \Omega_0 m_e c \sqrt{2J + m_e^2 c^2} - \omega J - qE_0 \left(\frac{J}{2}\right)^{1/2} \cos\psi, \tag{19}$$

which immediately yields Hamilton's equations

$$\frac{d\psi}{dt} = \frac{\Omega_0 m_e c}{\sqrt{2J + m_e^2 c^2}} - \omega - \frac{qE_0}{2\sqrt{2J}} \cos\psi, \tag{20}$$

$$\frac{dJ}{dt} = -qE_0 \left(\frac{J}{2}\right)^{1/2} \sin\psi. \tag{21}$$

These equations describe the motion seen in a frame rotating at a rate of ω . The fixed point (J_f, ψ_f) of the above equations can be found by setting $d\psi/dt = dJ/dt = 0$. From Eq. (21) we obtain $\psi_f = 0$ or π , and from Eq. (20)

$$\frac{\Omega_0 m_e c}{\sqrt{2J_f + m_e^2 c^2}} - \omega = \pm \frac{qE_0}{2\sqrt{2J_f}}. \tag{22}$$

The plus and minus signs on the right hand side correspond, respectively, to $\psi_f = 0$ and $\psi_f = \pi$. To determine the stability of a fixed point, we linearize Eqs. (20) and (21). If the eigenvalues of the linearized equations have imaginary (real) values, then the corresponding fixed point is stable (unstable) [1,10]. A straightforward analysis reveals that the fixed point is stable if

$$\frac{(qE_0)^2}{8J_f} - \frac{qE_0\Omega_0 m_e c \sqrt{2J_f}}{2(2J_f + m_e^2 c^2)^{3/2}} \cos\psi_f > 0. \tag{23}$$

It is helpful to plot Eq. (22) in a graph, as shown in Fig. 4, where parameter values are chosen such that $m_e = q = c = \Omega_0 = 1$, $\omega = 0.5$, and $E_0 = 0.25$ (in arbitrary units). The letters S and U indicate, respectively, that the point is stable or unstable. Note that at the present parameter values there are three fixed points, one of which is elliptic (stable, $\psi_f = \pi$), another central (stable, $\psi_f = 0$) and another hyperbolic (unstable, $\psi_f = 0$). Here one can immedi-

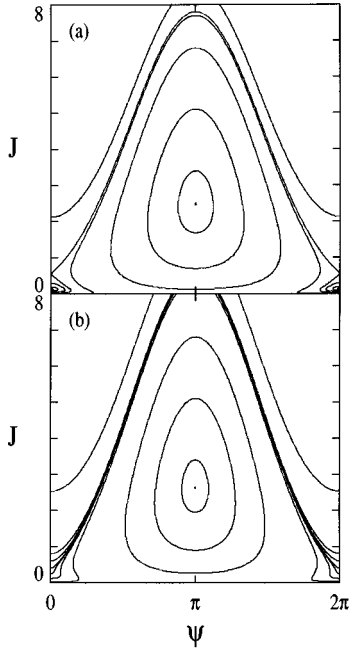


FIG. 5. Trajectories of the Hamiltonian (19) in (ψ, J) space for the same parameters as in Fig. 1. (a) At $E_0=0.4$, there are three fixed points: an elliptic fixed point at $(\pi, 2.47)$, a hyperbolic fixed point at $(0, 0.55)$, and a central fixed point at $(0, 0.13)$. (b) At $E_0=0.46$, there is one fixed point: an elliptic fixed point at $(\pi, 2.63)$.

ately predict that, if E_0 is increased above a certain value, the dotted curve ($\psi_f=0$) above the J axis will not cross the solid curve, meaning that the two fixed points (central and hyperbolic) will be lost. A simple calculation shows that the bifurcation occurs at the critical value of $E_0=0.45$, which agrees roughly with 0.433 that was previously determined from Fig. 3. To better understand the situation during the bifurcation, we numerically integrate Eqs. (20) and (21), and obtain Fig. 5. Figures 5(a) and 5(b) correspond, respectively, to the cases below and above the critical value of E_0 .

To improve the accuracy of the theoretical estimation of the critical value of E_0 , we need to go to higher-order perturbation theories such as Lie perturbation theories [19,20]. With the second term in the brackets of Eq. (15) back in its place, we perform a calculation to second order, and obtain the Hamiltonian

$$\begin{aligned} \bar{H}(\bar{I}, \bar{\theta}) = & \Omega_0 m_e c \sqrt{2\bar{I} + m_e^2 c^2} - \frac{(qE_0)^2}{8[\omega + \Omega(\bar{I})]} \\ & + \frac{(qE_0)^2 \bar{I} \frac{d\Omega(\bar{I})}{d\bar{I}}}{8[\omega + \Omega(\bar{I})]^2} - qE_0 \sqrt{\bar{I}/2} \cos(\bar{\theta} - \omega t), \end{aligned} \quad (24)$$

where

$$\Omega(\bar{I}) = \frac{\Omega_0 m_e c}{\sqrt{2\bar{I} + m_e^2 c^2}}, \quad (25)$$

and \bar{I} and $\bar{\theta}$ stand for the action and angle variables, respectively. In obtaining the above Hamiltonian using Lie perturbation theories, due consideration should be given to the first term in the brackets of Eq. (15). Since our interest is restricted to the region near the period-1 resonance, this term gives rise to secularity. Thus the first-order Hamiltonian should be chosen so as to eliminate the secular term. Once we obtain a Hamiltonian which is correct to second order, we can follow the same procedure represented by Eqs. (16)–(23). The improved critical value of E_0 so obtained is $E_0=0.432$, which is obviously in a good agreement with the one determined from Fig. 3.

We next wish to study the mechanism through which the second-order period-3 resonance is formed. It is known that a second-order resonance occurs when the frequency of the local motion around a primary resonance is rationally related with the driving frequency [10,12]. It therefore is important to know the behavior of the system near the primary period-1 resonance. The motion around the primary period-1 resonance can be effectively described by the Hamiltonian of Eq. (19). In particular, in the neighborhood of the period-1 elliptic fixed point, the Hamiltonian can be expanded to yield

$$H'(\delta J, \delta\psi) \cong -\frac{(\delta J)^2}{2M} - \frac{1}{2}K(\delta\psi)^2, \quad (26)$$

where

$$\frac{1}{M} = \frac{\Omega_0 m_e c}{(2J_f + m_e^2 c^2)^{3/2}} + \frac{qE_0 \sqrt{2}}{8J_f^{3/2}}, \quad (27)$$

$$K = qE_0 \left(\frac{J_f}{2} \right)^{1/2}. \quad (28)$$

The frequency of the local rotational motion just near the elliptic fixed point is then given by

$$\Omega'_f = \left(\frac{K}{M} \right)^{1/2} = \left[qE_0 \left(\frac{J_f}{2} \right)^{1/2} \left(\frac{\Omega_0 m_e c}{(2J_f + m_e^2 c^2)^{3/2}} + \frac{qE_0 \sqrt{2}}{8J_f^{3/2}} \right) \right]^{1/2}. \quad (29)$$

It should be noted that the motion around the elliptic fixed point is counter-clockwise, which is manifested by the minus signs in Eq. (26). A second-order resonance bifurcates out of the elliptic fixed point whenever the following resonance condition is met:

$$\frac{\Omega'_f}{\omega} = \frac{m}{n} \equiv \alpha, \quad (30)$$

where n and m are integers. Here the introduction of the concept of the rotation number α [1,10] turns out to be useful. In Fig. 1(c), the period-3 elliptic fixed point accompanying the second-order period-3 resonance completes its cycle clockwise around the period-1 elliptic fixed point every third period of the driving electric field, and the corresponding local rotation number is $\alpha = \frac{1}{3}$. Since we are now in a frame rotating at a rate ω , the local rotation number of the second-order resonance in this frame should be

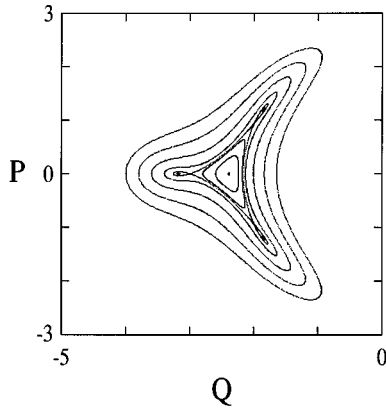


FIG. 6. Phase-space map after the birth of the second-order period-3 resonance for the same parameters as in Fig. 1, except $E_0=1.67$.

$$\alpha = \frac{1}{3} - 1 = -\frac{2}{3}, \quad (31)$$

where the minus sign in front of $2/3$ indicates that the corresponding motion is counterclockwise. Substituting Eqs. (29) and (31) into Eq. (30), we finally determine that the bifurcation occurs at the critical value of $E_0=1.65$. In Fig. 6, we present a phase-space map just after the birth of the second-order period-3 resonance.

V. CONCLUSION

We have investigated the relativistic dynamics of a charged particle in a uniform magnetic field and an oscillating electric field. It has been shown that, even though the corresponding nonrelativistic system yields simple integrable dynamics, the system can exhibit a variety of complex behaviors when relativistic effects become appreciable. For instance, nonlinear resonances, stochastic layers near separatrices, bifurcations of fixed points, and reconnection phenomena may occur in the system. All of these features originate from the relativistic nonlinearity, i.e., the nonlinearity in the relativistic kinetic energy term in the Hamiltonian. Thus it is evident that the relativistic nonlinearity alone can give rise to chaos.

From a practical viewpoint, we hope that the present work will contribute toward a better understanding of the relativistic dynamics of particles in an accelerator. It may also help to better understand the complex motion of an ion that may occur in the Fourier-transform ion cyclotron resonance mass spectrometry experiments [9].

ACKNOWLEDGMENTS

This research was supported by the Korea Science and Engineering Foundation (KOSEF) under Grant No. 961-0202-011-2, and by the Agency for Defense Development (ADD) of Korea.

APPENDIX

We wish to show that the variables Q and P of Eq. (8) are canonical variables. The Hamiltonian for our relativistic charged particle in a uniform magnetic field $\mathbf{B} = B\mathbf{e}_z$ and a

sinusoidal electric field $\mathbf{E} = E_0 \cos \omega t \mathbf{e}_y$ can be written as

$$H = \sqrt{m^2 c^4 + (\mathbf{p}' - q\mathbf{A})^2 c^2} + q\phi, \quad (A1)$$

where \mathbf{p}' is the canonical momentum given by

$$\mathbf{p}' = \mathbf{p} + q\mathbf{A}, \quad (A2)$$

and ϕ and \mathbf{A} are, respectively, scalar and vector potentials given by

$$\phi = -yE_0 \cos \omega t, \quad (A3)$$

$$\mathbf{A} = -yB\mathbf{e}_x. \quad (A4)$$

Substituting Eqs. (A3) and (A4) into Eq. (A1) and denoting the constants p'_x and p'_z by α and β , we obtain

$$H = \sqrt{m_e^2 c^4 + c^2(\alpha + qBy)^2 + c^2 p_y'^2} - qyE_0 \cos \omega t, \quad (A5)$$

where m_e is defined by

$$m_e^2 = m^2 + \beta^2/c^2. \quad (A6)$$

We now perform a canonical transformation from (y, p_y') to (Q', P') with a generating function of the second kind,

$$F_2(y, P', t) = \left(y + \frac{\alpha}{qB} \right) P' - \frac{\alpha E_0}{\omega B} \sin \omega t. \quad (A7)$$

The relation between (y, p_y') and (Q', P') is given by

$$p_y' = \frac{\partial F_2}{\partial y} = P', \quad (A8)$$

$$Q' = \frac{\partial F_2}{\partial P'} = y + \frac{\alpha}{qB}, \quad (A9)$$

and the resulting Hamiltonian is

$$\begin{aligned} H' &= H + \frac{\partial F_2}{\partial t} \\ &= \sqrt{m_e^2 c^4 + c^2(qBQ')^2 + c^2 P'^2} - qQ'E_0 \cos \omega t. \end{aligned} \quad (A10)$$

Finally, a scale transformation

$$Q = qBQ', \quad (A11)$$

$$P = P' \quad (A12)$$

yields the Hamiltonian

$$H'' = qBH' = \Omega_0 m_e^2 c^2 \sqrt{1 + (Q^2 + P^2)/m_e^2 c^2} - QqE_0 \cos \omega t, \quad (A13)$$

where $\Omega_0 = qB/m_e$. Equation (A13) is identical with Eq. (8). We have thus proved that the transformation from $(y, p_y' = p_y)$ to $(Q = qBQ' = qBy + p_x' = p_x, P = p_y' = p_y)$ is an extended canonical transformation.

- [1] E. Ott, *Chaos in Dynamical Systems* (Cambridge University Press, Cambridge, 1993).
- [2] A. E. Kaplan, Phys. Rev. Lett. **48**, 138 (1982).
- [3] G. Gabrielse, H. Dehmelt, and W. Kells, Phys. Rev. Lett. **54**, 537 (1985).
- [4] A. A. Chernikov, T. Tél, G. Vattay, and G. M. Zaslavsky, Phys. Rev. A **40**, 4072 (1989).
- [5] W. C. Schieve and L. P. Horwitz, Phys. Lett. A **156**, 140 (1991).
- [6] Y. Nomura, Y. H. Ichikawa, and W. Horton, Phys. Rev. A **45**, 1103 (1992).
- [7] J. H. Kim and H. W. Lee, Phys. Rev. E **51**, 1579 (1995); **52**, 473 (1995).
- [8] S. P. Drake, C. P. Dettmann, and N. E. Frankel, Phys. Rev. E **53**, 1351 (1996).
- [9] S. Guan, M. V. Gorshkov, G. M. Alber, and A. G. Marshall, Phys. Rev. A **47**, 2730 (1993).
- [10] A. J. Lichtenberg and M. A. Leiberman, *Regular and Stochastic Motion* (Springer-Verlag, New York, 1983).
- [11] C. F. F. Karney, Phys. Fluids **21**, 1584 (1978).
- [12] G. Corso and F. B. Rizzato, J. Plasma Phys. **49**, 425 (1993); Phys. Rev. E **52**, 3591 (1995).
- [13] C. Polymilis and K. Hizanidis, Phys. Rev. E **47**, 4381 (1993).
- [14] P. A. Lindsay and X. Chen, IEEE Trans. Plasma Sci. **22**, 834 (1994).
- [15] B. V. Chirikov, Phys. Rep. **52**, 263 (1979).
- [16] J. E. Howard and S. M. Hols, Phys. Rev. A **29**, 418 (1984); J. E. Howard and J. Humpherys, Physica D **80**, 256 (1995).
- [17] J. P. van der Weele and T. P. Valkering, Physica A **153**, 283 (1988).
- [18] D. del-Castillo-Negrete and P. J. Morrison, Phys. Fluids A **5**, 948 (1993).
- [19] B. McNamara, J. Math. Phys. **19**, 2154 (1978).
- [20] J. R. Cary, Phys. Rep. **79**, 129 (1981).